Boat Detection Using Visible Infrared Imaging Radiometer Suite in Philippine Waters

Anton Louise P. De Ocampo
College of Engineering
Batangas State University
Batangas City, 4200 Philippines
antonlouise.deocampo@ieee.org

Date received: January 5, 2023
Revision accepted: September 9, 2024

Abstract

The nighttime boat detection system utilizes the Day/Night Band (DNB) from the Visible Infrared Imaging Radiometer Suite (VIIRS) onboard the Suomi National Polar-orbiting Partnership (Suomi-NPP) Satellite. However, no locally developed algorithm exists for nighttime boat detection. This study aims to develop an algorithm that processes irradiance data from Suomi-NPP Science Data Records to extract boat locations based on nighttime lights. For the first time in Philippine waters, the study implemented a locally developed nighttime fishing boat detection system and recorded detections for potential temporal analysis of fishing activities. The process of generating the nighttime lights for boat detection involves several filtering steps to exclude extraneous features, such as flashes of lightning, moonlight, stray light, and high-energy atmospheric particles. The filtered radiance spikes and sharpness are then characterized to generate boat detections from the low-light data. Due to the absence of Automated Identification Systems (AIS) for marine vessels in the Philippines, the boat detection algorithm is tested on available AIS data from the Gulf of Mexico. The developed nighttime boat detection algorithm achieved a precision rate of 71.76% comparable to a commercially available system (75.06 %). The AIS and satellite data used for validation were timestamped on May 31, 2022, from 00:12 AM to 00:18 AM (Mexico Local Time). With this system integrated into local monitoring efforts, authorities will gain enhanced flexibility, allowing them to tailor the system to the community's needs. Ultimately, it complements the efforts of both local and global agencies in monitoring and educating the community on the responsible utilization of marine resources.

***Keywords**:* Day-Night Band, marine vessels monitoring**,** nighttime lights, remote sensing, satellite low-light imaging

---

1. Introduction

The use of nighttime lights for remote sensing applications has been made possible by the development of low-light-detecting satellites in the past few decades. The U.S. Defense Meteorology Satellite Program/Optical Line Scanner (DMSP/OLS) was the first satellite designed for nighttime detection, launching in 1973 and operating for over 40 years (Kumar *et al*., 2017; Pereira, 2002; Verma, 2016). The Visible Infrared Imaging Radiometer Suite (VIIRS) onboard the Suomi National Polar-orbiting Partnership (SNPP) represents a major improvement over its predecessor with its multispectral sensors and onboard calibration system (Xie *et al.*, 2014). The primary objective of the VIIRS instrument is to detect clouds using moonlight instead of sunlight, a fundamental requirement for meteorologists (Elvidge *et al.*, 2017). However, the benefits of the use of VIIRS low-light imaging extend far beyond meteorology. Numerous techniques and approaches have been applied to filter and process nighttime light satellite data, enabling its use in a wide range of applications and studies. These include natural water resources (Huang *et al*., 2016; Sheffield *et al*., 2018), city planning (Jiang *et al*., 2020; Cai *et al*., 2021), energy monitoring (Sun *et al*., 2020; Kong *et al.*, 2022), carbon modeling (Zhang *et al*., 2017), urban geography (Yang *et al*., 2019; Sharma *et al.*, 2016), ecology (Xu *et al.*, 2019), and demography (Xie *et al*., 2014).

Among the remote sensing applications of VIIRS, its use in boat detection emerged as a valuable tool in maritime security, fisheries management, and environmental protection. Researchers have employed different approaches to process the nighttime light data collected by the VIIRS instrument to detect boats. One approach involves feature engineering to identify the characteristics of the emitted light applying a rule-based classifier, often using thresholding to determine if the light originates from a boat. Another common approach is the use of machine learning or deep learning in classification.

The boat detection system developed by the Earth Observation Group (Elvidge *et al.*, 2015) employed a rule-based approach to classify nighttime lights as either lit boats or not. The science data records (SDRs) retrieved from the VIIRS instrument are stretched and scaled to render a grayscale image of the subject area at night. A series of filters enhances the intensity and distribution of light in the image. Thresholding the measurements of these intensity and distribution characteristics allows for the differentiation between boats and other sources of light. In addition to intensity and distribution, diffusion measurements can also be used as features for classifying nighttime lights, as proposed by Xue *et al*. (2022). The study of Kim *et al*. (2021) adopted a similar approach but incorporated moon phases to determine the thresholds used for classifying lit boats. In this study, the same set of features was used to characterize the nighttime lights, but an adaptive threshold based on sky conditions at different moon phases was applied rather than using an expert-identified threshold.

The machine learning approach primarily differs in the classifier used in boat detection, but similar features are extracted from the retrieved SDRs. In a study conducted by Tsuda *et al.* (2023), the feature vector generated to represent regions with lit boats includes Day/Night Band (DNB) radiance, spike median index, spike height index, maximum integer cloud mask, moon illumination, and zenith angles of the satellite, the moon, and the sun. The Random Forest (RF) algorithm is then used for classification. However, this feature extraction process can be automated using deep learning techniques, as proposed by Shao *et al.* (2021), where automated feature extraction occurs in convolutional neural networks (CNN) in a small-object detection model.

Several studies on boat detection systems using VIIRS low-light images focus on waters surrounding Japan (Liu *et al.*, 2015), Indonesia (Elvidge *et al*., 2018), China (Shi and Wang, 2018), the Philippines (Geronimo *et al*., 2018), Arabian regions (Sarangi and Narayanan, 2021), and others. Although a study on fishing boat detection was conducted in Philippine waters by Geronimo *et al*. (2018), they used the commercial boat detection system provided by Earth Observation Group (Elvidge *et al.*, 2015).

The Philippines, with its vast archipelago of more than 7,000 islands, encompasses a diverse marine environment that includes calm waters and rough waters shaped by monsoonal winds and ocean dynamics (Boquet, 2017). Navigating the region presents challenges due to its varied geology and frequent weather disturbances, despite its strategic location along major international shipping routes. Additionally, the Philippines' abundant fishing grounds are vital to its maritime activities and have a significant economic impact on the country and its coastal communities. However, the fishing sector faces challenges like overfishing and environmental degradation, highlighting the need for sustainable management techniques (Liu *et al*., 2021). One critical piece of management information that could help monitoring agencies is the characterization of shipping and fishing activities using boat detection systems.

At the time of writing, no locally developed algorithm exists for nighttime boat detection in the Philippines. This study aims to develop an algorithm that processes irradiance data from Suomi-NPP Science Data Records to extract boat locations based on nighttime lights. For the first time in Philippine waters, this study implemented a locally developed nighttime fishing boat detection system and recorded these detections for potential temporal analysis of fishing activities.

2. Methodology

The VIIRS DNB Boat Detection algorithm aims to estimate the total number of lit boats or marine vessels during nighttime. Figure 1 summarizes the algorithm for boat detection. The process starts with the input of Science Data Records (SDRs), which contain the sensor readings retrieved from the VIIRS instrument, which is available at NASA's LAADS-DAAC (Level-1 and Atmosphere Archive & Distribution System Distributed Active Archive Center, n.d.). The SDR is reoriented to align with the subsequent processing, which includes both linear and logarithmic scaling. Scaling adjusts the data range of the sensor measurements. To smooth out the data after scaling, Weiner and median filters were applied. The algorithm simultaneously detects lightning to differentiate between boat lights and natural lightning. Filtered data is subtracted to highlight significant features such as spikes indicative of potential boat detections. The relative height of these spikes is measured to distinguish stronger signals, such as boats, from weaker ones. An S3 sharpness indexing step assesses the sharpness of the detected spikes to further refine the classification. Finally, the algorithm classifies the spikes based on characteristics such as height and sharpness, generating a list of detected boats.

Out of the 15 data products retrieved from VIIRS onboard the Suomi-NPP satellite, the VNP02DNB and VNP03DNB SDRs were selected for this study. The data fields from these SDRs, which represent the radiance DNB data and the geographic information, have been reoriented to match the conventional North. Due to the very low radiance measurements, both linear and logarithmic scaling are employed. At this stage, the SDR can be treated as a grayscale image.

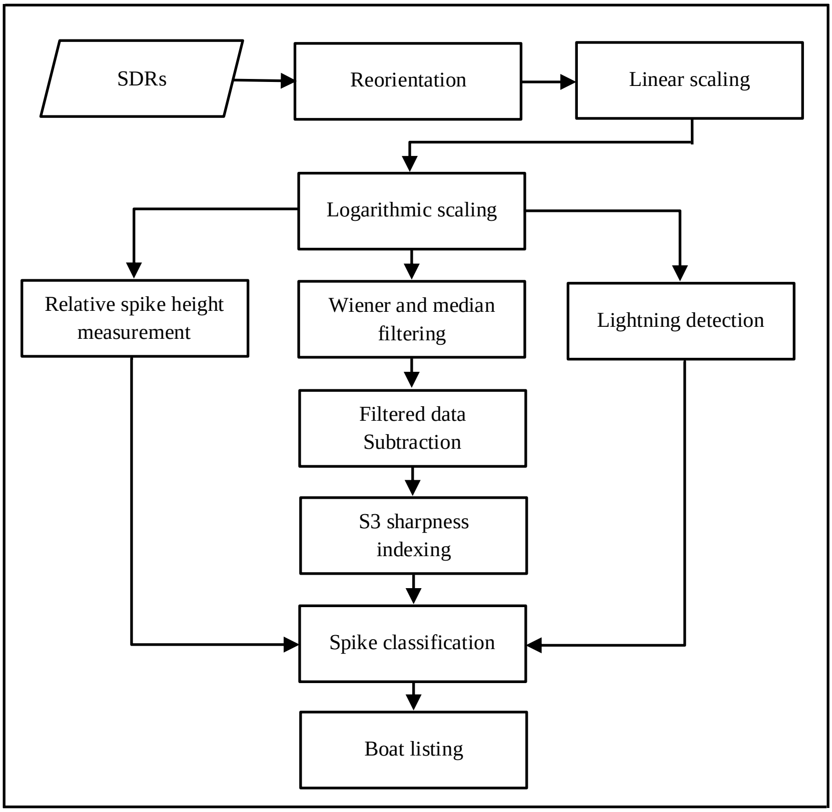

Figure 1. Overview of the boat detection algorithm from data acquisition to final detection, including preprocessing, feature extraction, and classification

2.1 Data

The core algorithm ingests sensor data records (SDRs), specifically the VNP02DNB and VNP03DNB data from the VIIRS instrument onboard the Suomi National Polar-orbiting Partnership (SNPP) satellite, downloaded through the Level-1 and Atmosphere Archive & Distribution System Distributed Active Archive Center (LAADS DAAC). The VNP02DNB and VNP03DNB are the L1B data generated from a 6-minute granule covered by SNPP, containing radiance observations and geolocation data, respectively. At the nadir, the DNB, which is categorized as an M-band, has a spatial resolution of 750 meters for the full scan. The panchromatic DNB operates in the 0.5 μm to 0.9 μm spectral range, which is useful for capturing night lights and solar and lunar reflections. It displays a wide dynamic range, ranging from quarter-moon illumination to bright daylight. The VNP03DNB data holds the line-ofsight (LOS) vectors for the single panchromatic Day-Night band (DNB). To generate these vectors, the geolocation algorithm relies on inputs such as the SNPP platform's ephemeris and attitude data, VIIRS sensor and satellite geometry, Earth ellipsoid, geoid, and digital terrain model. Each pixel in the VIIRS L1 image corresponds to geodetic coordinates (latitude and longitude) as well as additional information provided by the VNP03DNB including latitude, longitude, surface height above the geoid, solar, lunar, and sensor zenith and azimuth angles, land/water mask, moon illumination fraction and phase angle, and a quality flag for each pixel location. These SDRs are ingested into the VIIRS DNB algorithm to map lights on the earth's surface, followed by filtering to remove the noise from atmospheric phenomena such as lightning and ionospheric particle discharges. The strongest light intensities are assumed to be fishing vessels, as these boats use lights for navigation to attract prey. The SDR is downloaded in NetCDF (.nc) file format. Figure 2 shows the file attributes associated with the SDR. The file attributes show the multidimensional structure of the science data. The file was created on May 7, 2021, and is titled "VIIRS Day/Night Band Data," identified by the short name "VNP02DNB." The long name describes the data product in detail: "VIIRS/NPP Day/Night Band 6-Min L1B Swath 750m," indicating a Level 1B data product with a 750-meter resolution. The data originates from the VIIRS instrument onboard the Suomi National Polar-orbiting Partnership (NPP) satellite, which captures imagery in visible and infrared wavelengths.

```
Source:
        I:\My Drive\Work\Publications\For Publication\Submitted\VIIRS - MJST\VNP02DNB.A2020241.1606.002.2021127044400.nc
Format:
        netcdf4
Global Attributes:
        date_created                = '2021-05-07T00:44:42Z'
        ProductionTime              = '2021-05-07T00:44:42Z'
        title                       = 'VIIRS Day/Night Band Data'
        ShortName                   = 'VNP02DNB'
        LongName                    = 'VIIRS/NPP Day/Night Band 6-Min L1B Swath 750m'
        instrument                  = 'VIIRS'
        processing_version          = 'v3.0.0'
        Conventions                 = 'CF-1.6'
        institution                 = 'NASA Goddard Space Flight Center, VIIRS L1 Processing Group'
        license                     = 'http://science.nasa.gov/earth-science/earth-science-data/data-information-policy/'
        naming_authority            = 'gov.nasa.gsfc.VIIRSland'
        keywords_vocabulary         = 'NASA Global Change Master Directory (GCMD) Science Keywords'
```

Figure 2. Global attributes of the VIIRS/NPP Day/Night Band Moderate Resolution Terrain-Corrected Geolocation 6-Min L1 Swat 750m (VNP03DNB) Science Data Records file

2.2 SDR Processing

The collected SDRs are reoriented first before any signal processing. This reorientation process is identical to the transpose operation in matrices, which is necessary due to the arrangement of the detectors in the VIIRS instrument. Linear and logarithmic scaling are performed to enhance the relative differences between the values in the DNB data aggregates and to address the skewness of the DNB observations toward the very few high-intensity detections. After scaling, the DNB radiance data undergo Wiener and Median filtering. The Wiener filter is used to reduce noise (Chen *et al.*, 2006) in the observation data across the swath corresponding to the 6-minute granule. The median filter is employed to de-spike the DNB radiance data. This filter operates on a 3x3 pixel neighborhood, arranging the pixels in numerical order replacing the original value with the fifth position as the new value (Singh *et al.*, 2011).

The filtered data is then subtracted from the original DNB radiance. Afterward, all pixels with values lower than 0.035 after subtraction are discarded. The purpose of this subtraction is to emphasize the local maxima within clusters of spikes, as a lit boat appears as a single spot in the radiance data. The difference between this spot and other points in the cluster should be significant. The threshold of 0.035 was determined through multiple trials to effectively remove the clustered spots in the radiance data.

Following the subtraction, the spike height, or radiance relative to adjacent pixels, is measured as calculated using Equation 1.

$$s = \frac{2r_i - (r_{i-1} + r_{i+1})}{2r_i} \quad (1)$$

Where, s represents the relative height of the radiance of a pixel r_i against the two adjacent pixels, r_{i-1} *and* r_{i+1}. The value of s provides insight into the local difference between a spike to its proximity.

The measurement of the relative height of spikes allows the use of a threshold $s = 0.75$ to separate the strong boat detections from the weaker ones. Also, pixels with $s > 0.995$ and radiance of more than 1000 nanowatts are considered ionospheric discharges and discarded in the detection.

Radiances affected by clouds often exhibit some degree of blur. Quantifying this blur can aid in classifying spikes for boat detection. The sharpness measurement algorithm adopted in this study is the S3 mapping, which combines both the spectral and spatial sharpness measurements (Vu and Chandler, 2009). The same parameter configuration was applied, including a block size of 32, an overlap of 24 pixels, and a slope of 0.5. The threshold between blurry detections (QF3) and clear detections (QF1 or QF2) is set at a sharpness index of 0.4.

2.3 Lightning Detection

In addition to clouds, the DNB observations can also be affected by lightning flashes. These flashes are abrupt and can be detected simultaneously by the 16 detectors in the VIIRS instrument. The lightning detection method used in this study takes advantage of this and uses the radiance differences in adjacent scans. If the difference is substantial and persists across 24 or more pixels, then those detections are classified as lightning. In this study, the difference is considered substantial if it exceeds 10% of the higher reading between the two compared pixels.

2.4 Validation

The performance of the boat detection algorithm is cross-referenced with existing systems and data from the Automatic Identification System (AIS) for marine vessels. Figure 3 illustrates the validation workflow for the boat detection algorithm. Three datasets are collected for the validation process: the boat detections from a commercial and existing boat detection algorithm, AIS records, and the raw SDR file from the LAADS-DAAC archive. The results of the boat detections from the proposed algorithm are cross-referenced with those from the existing algorithm and AIS records.

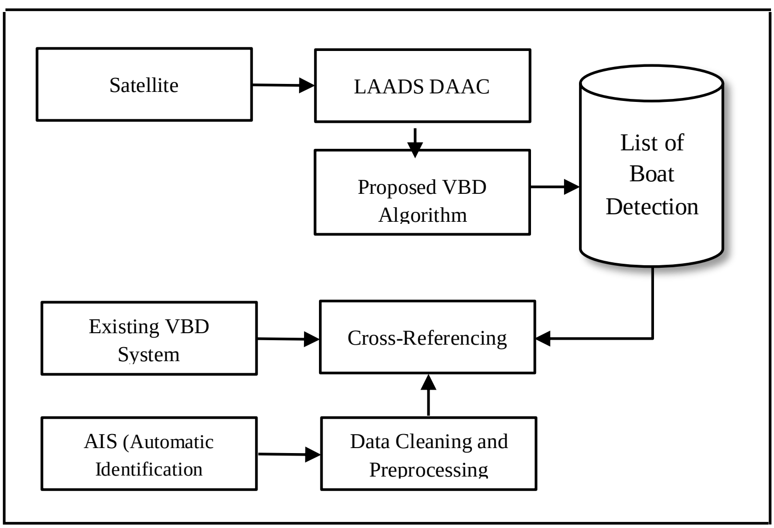

Figure 3. Validation workflow for the boat detection algorithm using three datasets: commercial algorithm detections, AIS records, and raw SDR files from the LAADS DAAC archive

The Earth Observation Group (Elvidge *et al.*, 2015) pioneered the use of VIIRS DNB data for detecting lit boats used in fishing. Their detection algorithm's results were available for free until May 31, 2022, after which subsequently became accessible via subscription. The nightly data could be downloaded in CSV and KMZ formats viewable on Google Earth, and users could select results based on specific regions. AIS uses a transponder system designed for the exchange of information between ships, and between ship and shore stations. Its goals include aiding in vessel identification, target tracking, information simplification, information interchange, and providing new data to improve situational awareness. AIS is based upon a technology called "Self-Organized Time Division Multiple Access - SOTDMA" which allows for seamless operation worldwide.

The limited available AIS data poses a challenge for validating the results of the VBD algorithm, as the initially selected region of interest was the Philippines. Data from the Synthetic Aperture Radar and Automatic Identification System for Innovative Terrestrial Monitoring and Maritime Surveillance (SAR with AIS) Project by DOST ASTI is limited, necessitating the use of another region for validation. Fortunately, the National Oceanic and Atmospheric Administration (NOAA) has an office for coastal management that features the digital coast "Marine Access AIS", which contains data about ocean vessel detection and identification from 2009 to the present. Since NOAA's Marine Access AIS is exclusive to US coasts, the region covering the Gulf of Mexico was used for validation.

3. Results and Discussion

The generated output of the algorithm includes the coordinates of the detected boat detection from the DNB aggregate and the visualization file that can be viewed in Google Earth and GIS mapping tools.

The area presented in Figure 4 is the Philippine region, bounded to the North at 23.9591˚ Lat, South at -0.88792˚ Lat, East at 138.2559˚, and West at 105.3105˚. However, georeferencing the observation data requires reorientation, as the DNB data (Figure 4a) is transposed about the arrangement of detectors in the VIIRS and the direction of the scan. To validate the orientation correction, the Black Marble image (Figure 4b) covering the Philippines was used as a reference. A sample orientation-corrected DNB observation data is presented in Figure 4c. The original observation data should be flipped vertically and rotated 90° clockwise or transposed.

In its initial form, the observation data is incomprehensible due to the very low radiance measured at nighttime (Figure 5a). To augment this, the observation data is multiplied by 10^9, translating the initial measurement from $W/cm^2/sr$ to $nW/cm^2/sr$ (Figure 5b). Due to the very high dynamic range of VIIRS (specifically 10^7), an 8-bit RGB image cannot render the differences between very low radiances. Because spikes are quite few compared to the low radiances that represent the bulk of the observation data, it is necessary to express the DNB observations on a logarithmic scale (Figure 5c).

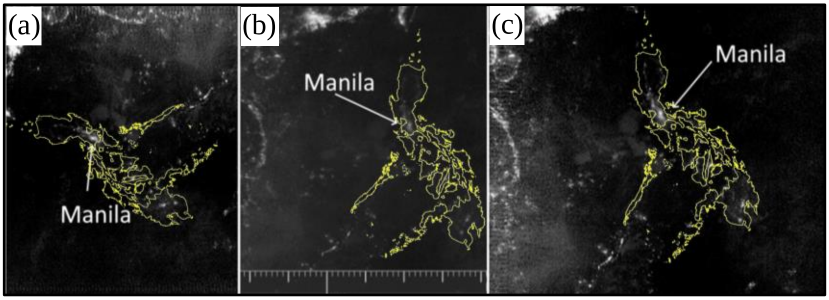

Figure 4. DNB observation data from SNPP VIIRS Granule (a); from NASA Black Marble via World View (b); Reoriented DNB observation data (c)

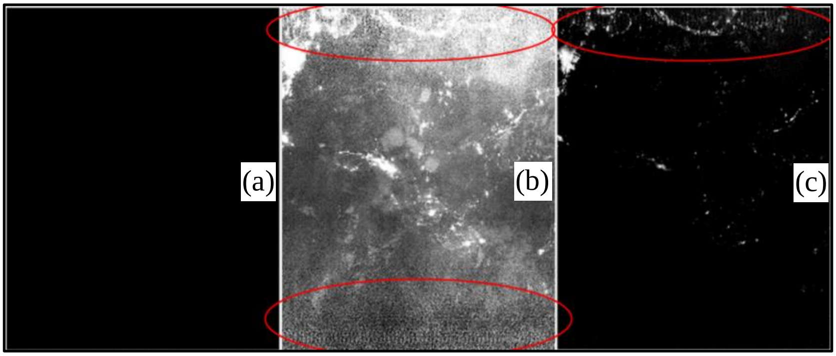

Figure 5. DNB radiance in $W/cm^2/sr$ (a); DNB radiance in $nW/cm^2/sr$ (b); logarithm of DNB radiance. The red marks show the noise generated by aggregating the readings of the VIIRS detectors (c)

During a single scan, the detectors in the VIIRS instrument sweep out a swath between -56.28° and +56.28° scan angles. Because of the "bow-tie" effect (Seaman *et al*., 2015), it is necessary to perform sub-pixel aggregation in both the scan and track directions. There are 32 distinct modes in the DNB sample aggregation as a function of the scan angles. The software aggregation in the VIIRS instrument results in the noise present near the edge of each swath, as shown in Figure 5 with red marks. The best signal-to-noise ratio can be observed in the nadir portion of the scan. The use of the Wiener filter flattens this aggregation noise across the entire swath. Since lit boats appear as spikes in the DNB observation data, the local maxima can be identified by de-spiking the DNB observation data and subtracting it from the original. Then, by applying a threshold to the resulting difference, clustered spikes can be removed since lit boats appear to be individual spots in DNB observation data. Figures 4 and 5 show the unmasked DNB observations. However, at the start of feature extraction, the DNB observations were subjected to the land/water masks included in the Sensor Data Records (SDR) retrieved from VIIRS instruments. Figure 6 shows a region in the West Philippine Sea. The image on the left displays the Wiener- and median-filtered DNB radiance data, while the right is the result of the subtraction. It clearly illustrates the removal of clustered spikes by considering only the local maxima.

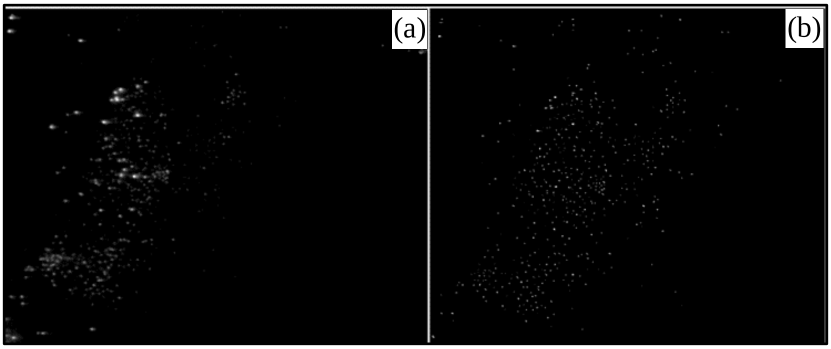

Figure 6. Median and Wiener-filtered (a); difference from the original DNB observation data (b)

Boat detection primarily considers the characteristic of lighting as spikes in the radiance data, which covers approximately a single pixel. Note that the DNB resolution per pixel is about 750 m, which can only represent a single spike that has a greater intensity than the other adjacent pixels. The intuition for quantifying the height of a spike relative to adjacent ones is that if the subject pixel represents a lit boat, the average intensity of adjacent pixels is significantly less than that of the subject pixel. However, if the subject pixel's intensity is almost the same as the average of the adjacent pixels, and their intensity measures greater than 1 milliwatt, the subject pixel is considered an ionospheric discharge and is discarded from the boat detections.

Measuring the attributes of a spike relative to its surroundings allows for the classification of that radiance into categories of boat detection. Figure 7 presents the relative height of spikes used to separate strong boat detections from weaker ones.

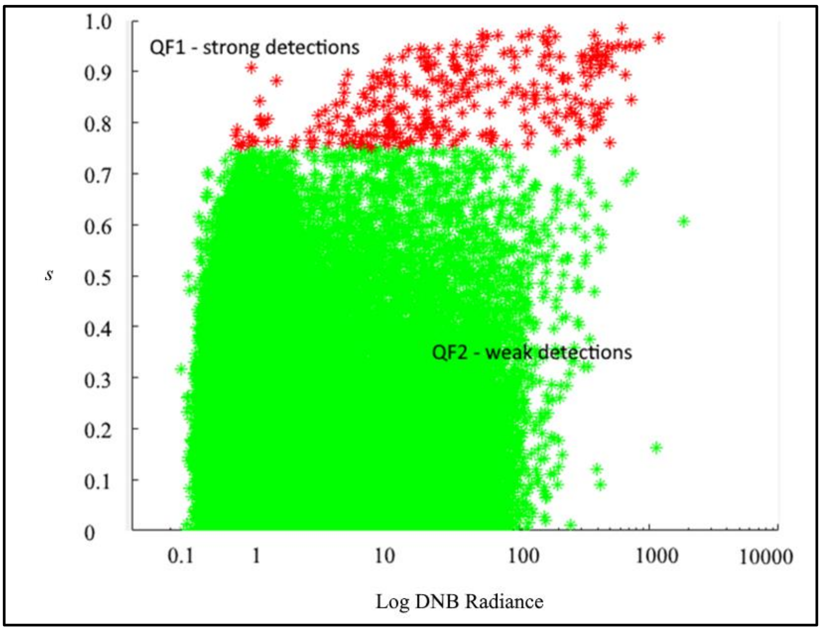

Figure 7. Relative height of spikes used to distinguish strong boat detections from weaker ones.

Clouds affect the radiances of lit boats seen from space. Fortunately, sharpness measurements can quantify the blur incurred in the radiances detected. By considering both spatial and spectral sharpness of the image derived from the DNB observations, the blur can be removed, emphasizing the sharp pixels. Figure 8 shows the DNB observations with clouds present (Figure 8a) and the result of employing sharpness measurement (Figure 8b).

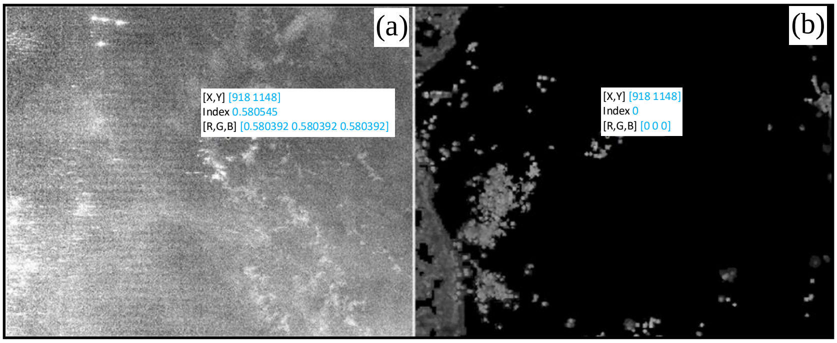

Figure 8. DNB radiance in nW/cm^2/sr (a); the sharpness measurements emphasize the sharp blocks (b)

During nighttime, multiple sources of light overshadow the lit boats offshore. These stray lights include ionospheric particles and lightning. The lightning detection algorithm is crucial to boat detection at night, as it helps discard the pixels influenced by lightning. This detection capitalizes on the fact that persistent occurrences can be detected simultaneously by the 16 detectors in the VIIRS instrument. A set of 16 simultaneous readings is referred to as a segment in this paper. A difference of more than 0.1 log (DNB) between adjacent segments, along with persistence across 24 pixels or more, is considered lightning. In Figure 9, the detected lightning appears as a strip of light, which is discarded in the classification of the boat detections.

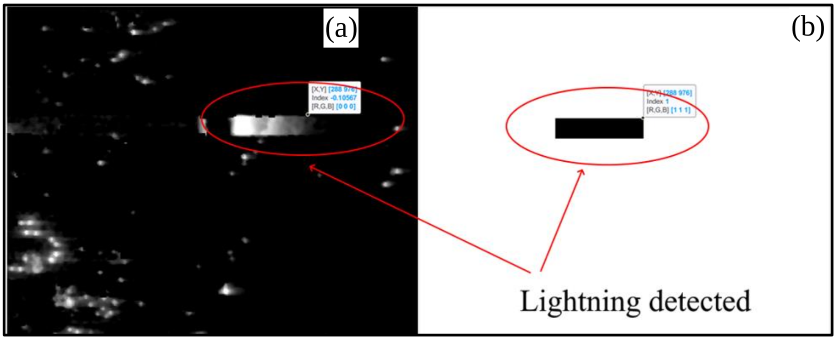

Figure 9. Lightning creates a white strip with exactly 16 lines in width, in the DNB radiance image (a); the pixels influenced by lightning are discarded in the boat detection (b)

The results of filtering, sharpness mapping, lightning detection, and relative height measurements are used to classify the radiances into different classes of detection from strong to weak, lightning or ionospheric particle discharge, and blurry detections.

The results of the boat detection algorithm are cross-referenced to the existing boat detection system (Elvidge *et al.*, 2015) and the data from the Automatic Identification Systems (AIS) used in marine vessel monitoring. The detection performance of the proposed algorithm is measured based on its ability to estimate the precise location of each identified boat. However, the AIS dataset includes many boats, including non-lit boats and non-fishing vessels, resulting in a significantly higher missing alarm rate than would be expected in practice, leading to an impractical recall rate (R). As a result, when evaluating the detection findings using AIS data, only the precision (P) is taken into account.

The limited availability of AIS data poses a challenge for validating the results of the VBD algorithm, since there is no comprehensive AIS implementation in the Philippines at the time of the study. To address this, data from Marine Access AIS provided by the National Oceanic and Atmospheric Administration (NOAA) covering the Gulf of Mexico was used for validation. The highest precision obtained when comparing the proposed algorithm to the AIS data from the Gulf of Mexico is 71.76%. However, this precision is quite close to that of the existing boat detection algorithm, which achieves a precision rate of 75.06% when compared with the same AIS data. Figure 10 presents a sample visualization of the detections from the existing algorithm (Figure 10a) and the proposed (Figure 10c), along with the boat listings from the AIS data.

The developed boat detection algorithm was implemented to scan Philippine waters. Figure 11 provides a sample of the detections exported to the Google Earth browser. Each boat is represented by a blue sailing ship icon with corresponding coordinates labeled. Every observed vessel includes a description with the date it was spotted, its precise coordinates, and its fishery management area (FMA). As of May 31, 2022, 288 vessels were traveling within Philippine territorial waters. The highest concentration of fishing boats was found in the waters surrounding the Zamboanga peninsula in Western Mindanao, the Philippines, and the Kalayaan Group of Islands in the West Philippine Sea.

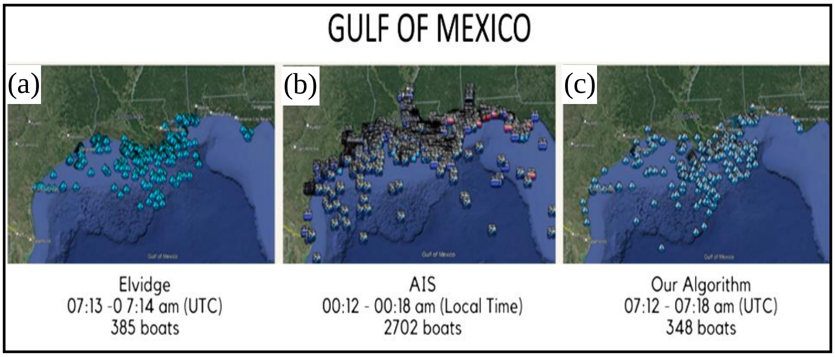

Figure 10. Visualization of the existing boat detection (Elvidge *et al.*, 2015) (a); the data from Marine Access AIS(b); and the proposed algorithm (c)

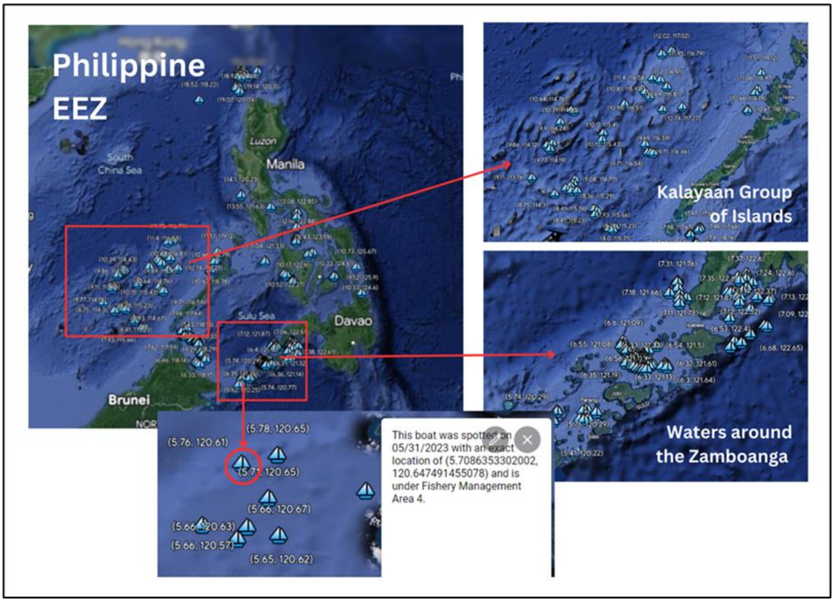

Figure 11. Implementation of the boat detection algorithm within the Philippine Exclusive Economic Zone (EEZ).

The proposed boat detection algorithm is still under development for its potential application in promoting sustainable fishing. The local capacity for boat detection provides temporal data from the aggregation of detections over a certain period, which can reveal the behavior and density of fishing activities. This information on fishing efforts can assist local authorities in identifying overfished regions and recommending other fishing areas to fisherfolks and commercial fishermen. Moreover, in the absence of an Automatic Identification System (AIS), the results of the boat detection algorithm can provide invaluable insights into the frequency of fishing activities occurring in Philippine waters over time.

4. Conclusion and Recommendation

In the absence of an Automatic Identification System (AIS), the locally developed boat detection algorithm is introduced. The fishing boat detection algorithm developed in this study performs on par with existing systems and is the first of its kind implemented locally. The system offers several inherent advantages. First, the detections results are written in .csv and .kml formats, which can be viewed in any geographic information system software such as Google Earth, QGIS, etc. With such a system integrated into the local monitoring efforts, there will be enhanced flexibility that authorities can tailor to the community's needs. Ultimately, it complements the efforts of both local and global agencies in monitoring and educating the community on the responsible utilization of marine resources.

In future work, a localized validation study can be performed using a complementary localized AIS to strengthen the validity of the detection in Philippine waters. Additionally, the results of the lit boat detection system will be aggregated across year-long monitoring to identify the fishing behavior, which can help identify the overfished areas and recommend underfished regions.

5. Acknowledgement

This work was supported in part by the Philippine Space Agency (PhilSA) and the USAID Fishright program.

6. References

Boquet, Y. (2017). Environmental Challenges in the Philippines. In The Philippine Archipelago (pp. 779-829). Cham: Springer. https://doi.org/10.1007/978-3-319-51926-5_22

Cai, M., Shi, Y., Ren, C., Yoshida, T., Yamagata, Y., Ding, C., & Zhou, N. (2021). The need for urban form data in spatial modeling of urban carbon emissions in China: A critical review. Journal of Cleaner Production, 319, 128792. https://doi.org/10.1016/j.jclepro.2021.128792

Chen, J., Benesty, J., Huang, Y., & Doclo, S. (2006). New insights into the noise reduction Wiener filter. IEEE Transactions on audio, speech, and language processing, 14, 1218–1234. https://doi.org/10.1109/TSA.2005.860851

Elvidge, C.D., Baugh, K., Zhizhin, M., Hsu, F.C., & Ghosh, T. (2017). VIIRS night-time lights. International Journal of Remote Sensing, 38(21), 5860–5879. https://doi.org/10.1080/01431161.2017.1342050

Elvidge, C.D., Ghosh, T., Baugh, K., Zhizhin, M., Hsu, F.C., Katada, N.S., Penalosa, W., Hung, B.Q. (2018). Rating the effectiveness of fishery closures with visible infrared imaging radiometer suite boat detection data. Frontiers in Marine Science, 5, 132. https://doi.org/10.3389/fmars.2018.00132

Elvidge, C.D., Zhizhin, M., Baugh, K., & Hsu, F.C. (2015). Automatic boat identification system for VIIRS low light imaging data. Remote sensing, 7(3), 3020–3036. https://doi.org/10.3390/rs70303020

Geronimo, R.C., Franklin, E.C., Brainard, R.E., Elvidge, C.D., Santos, M.D., Venegas, R., & Mora, C. (2018). Mapping fishing activities and suitable fishing grounds using nighttime satellite images and maximum entropy modeling. Remote Sensing, 10(10), 1604. https://doi.org/10.3390/rs10101604

Huang, C., Chen, Y., Zhang, S., Li, L., Shi, K., & Liu, R. (2016). Surface water mapping from Suomi NPP-VIIRS imagery at 30 m resolution via blending with Landsat data. Remote Sensing, 8(8), 631. https://doi.org/10.3390/rs8080631

Jiang, Z., Zhai, W., Meng, X., & Long, Y. (2020). Identifying shrinking cities with NPP-VIIRS nightlight data in China. Journal of Urban Planning and Development, 146(4), 04020034. https://doi.org/10.1061/(ASCE)UP.1943-5444.0000598

Kim, E., Kim, S. W., Jung, H.C., & Ryu, J.H. (2021). Moon phase-based threshold determination for VIIRS boat detection. Korean Journal of Remote Sensing, 37(1), 69-84. https://doi.org/10.7780/kjrs.2021.37.1.6

Kong, X., Wang, X., Jia, M., & Li, Q. (2022). Estimating the Carbon Emissions of Remotely Sensed Energy-Intensive Industries Using VIIRS Thermal Anomaly-Derived Industrial Heat Sources and Auxiliary Data. Remote Sensing, 14(12), 2901. https://doi.org/10.3390/rs14122901

Kumar, P., Sajjad, H., Alare, R. S., Elvidge, C.D., Ahmed, R., & Mandal, V.P. (2017). Analysis of urban population dynamics based on residential buildings volume in six provinces of Pakistan using operational linescan system sensors. IEEE Sensors Journal, 17(6), 1656–1662. https://doi.org/10.1109/JSEN.2017.2652720

Level-1 and atmosphere archive & distribution system distributed active archive center. (n.d.). LAADS DAAC. Retrieved August 28, 2021, from https://ladsweb.modaps.eosdis.nasa.gov/

Liu, J.M., Borazon, E.Q., & Muñoz, K.E. (2021). Critical problems associated with climate change: a systematic review and meta-analysis of Philippine fisheries research. Environmental Science and Pollution Research, 28(36), 49425-49433. https://doi.org/10.1007/s11356-021-15712-6

Liu, Y., Saitoh, S.I., Hirawake, T., Igarashi, H., & Ishikawa, Y. (2015). Detection of squid and pacific saury fishing vessels around Japan using VIIRS Day/Night Band image. Proceedings of the Asia-Pacific Advanced Network, 39, 28-39. http://dx.doi.org/10.7125/APAN.39.3

Pereira, G.M. (2002). Investigations of fire dynamics in seasonally dry regions of the Amazon rainforest. University of Minnesota.

Seaman, C., Hillger, D.W., Kopp, T.J., Williams, R., Miller, S., & Lindsey, D. (2015). Visible Infrared Imaging Radiometer Suite (VIIRS) Imagery Environmental Data Record (EDR) user's guide. http://doi.org/10.7289/V5/TR-NESDIS-150

Shao, J., Yang, Q., Luo, C., Li, R., Zhou, Y., & Zhang, F. (2021). Vessel detection from nighttime remote sensing imagery based on deep learning. IEEE Journal of Selected Topics in Applied Earth Observations and Remote Sensing, 14, 12536-12544. https://doi.org/10.1109/JSTARS.2021.3125834

Sharma, R.C., Tateishi, R., Hara, K., Gharechelou, S., & Iizuka, K. (2016). Global mapping of urban built-up areas of year 2014 by combining MODIS multispectral data with VIIRS nighttime light data. International Journal of Digital Earth, 9, 1004–1020. https://doi.org/10.1080/17538947.2016.1168879

Sheffield, J., Wood, E.F., Pan, M., Beck, H., Coccia, G., Serrat-Capdevila, A., & Verbist, K. (2018). Satellite remote sensing for water resources management: Potential for supporting sustainable development in data-poor regions. Water Resources Research, 54, 9724–9758. https://doi.org/10.1029/2017WR022437

Shi, W. & Wang, M. (2018). Ocean dynamics observed by VIIRS day/night band satellite observations. Remote Sensing, 10(1), 76. https://doi.org/10.3390/rs10010076

Singh, S. (2011). An alternate algorithm for (3x3) median filtering of digital images. International Journal of Computers & Technology, 1(1), 7–9. https://doi.org/10.24297/ijct.v1i1.6732

Sun, S., Li, L., Wu, Z., Gautam, A., Li, J., & Zhao, W. (2020). Variation of industrial air pollution emissions based on VIIRS thermal anomaly data. Atmospheric research, 244(1), 105021. https://doi.org/10.1016/j.atmosres.2020.105021

Tsuda, M.E., Miller, N.A., Saito, R., Park, J., & Oozeki, Y. (2023). Automated VIIRS boat detection based on machine learning and its application to monitoring fisheries in the East China Sea. Remote Sensing, 15(11), 2911. https://doi.org/10.3390/rs15112911

Verma, S. (2016). Effect of forest fire on tree diversity, biomass and soil properties in a tropical dry deciduous forest of Western Ghats, India. (Dissertation). Department of Ecology & Environmental Sciences, School of Life Sciences, Pondicherry University, Puducherry, India.

Vu, C.T., & Chandler, D.M. (2009). S3: A spectral and spatial sharpness measure. MMEDIA '09: Proceedings of the 2009 First International Conference on Advances in Multimedia, (pp. 37–43). https://doi.org/10.1109/MMEDIA.2009.15

Xie, Y., Weng, Q., & Weng, A. (2014). A comparative study of NPP-VIIRS and DMSP-OLS nighttime light imagery for derivation of urban demographic metrics. 2014 Third International Workshop on Earth Observation and Remote Sensing Applications (EORSA), Changsha, China, 335–339. https://doi.org/10.1109/EORSA.2014.6927907

Xu, P., Wang, Q., Jin, J., & Jin, P. (2019). An increase in nighttime light detected for protected areas in mainland China based on VIIRS DNB data. Ecological Indicators, 107, 105615. https://doi.org/10.1016/j.ecolind.2019.105615

Xue, C., Gao, C., Hu, J., Qiu, S., & Wang, Q. (2022). Automatic boat detection based on diffusion and radiation characterization of boat lights during night for VIIRS DNB imaging data. Optics Express, 30(8), 13024-13038. https://doi.org/10.1364/OE.455555

Yang, C., Yu, B., Chen, Z., Song, W., Zhou, Y., Li, X., & Wu, J. (2019). A spatial-socioeconomic urban development status curve from NPP-VIIRS nighttime light data. Remote Sensing, 11(20), 2398. https://doi.org/10.3390/rs11202398

Zhang, X., Wu, J., Peng, J., & Cao, Q. (2017). The uncertainty of nighttime light data in estimating carbon dioxide emissions in China: A comparison between DMSP-OLS and NPP-VIIRS. Remote Sensing, 9(8), 797. https://doi.org/10.3390/rs9080797

Sarangi, R.K., & Narayanan, N.J.S. (2022). VIIRS boat detection (VBD) product-based night time fishing vessels observation in the Arabian Sea and Bay of Bengal Sub-regions. Geocarto International, 37(12), 3504-3519. https://doi.org/10.1080/10106049.2021.1878290